IUST
Iran University of Science and Technology

Iranian Journal of Electrical and Electronic Engineering

Journal Homepage: ijeee.iust.ac.ir

Precise Loss Estimation and Comprehensive Thermal Analysis of Axial-Field Flux-Switching PM Machine

A. Zarghani*, P. Dehgoshaei*, H. Torkaman*(C.A.), and A. Ghaheri*

Abstract: Losses in electric machines produce heat and cause an efficiency drop. As a consequence of heat production, temperature rise will occur which imposes severe problems. Due to the dependence of electrical and mechanical performance on temperature, conducting thermal analysis for a special electric machine that has a compact configuration with poor heat dissipation capability is crucial. This paper aims to carry out the thermal analysis of an axial-field flux-switching permanent magnet (AFFSPM) machine for electric vehicle application. To fulfill this purpose, three-dimensional (3D) finite element analysis is performed to accurately derive electromagnetic losses in active components. Meanwhile, copper losses are calculated by analytic correlation in maximum allowable temperature. To improve thermal performance, cooling blades are inserted on the frame of AFFSPM, and 3D computational fluid dynamics (CFD) is developed to investigate thermal analysis. The effect of different housing materials, the external heat transfer coefficient, and various operating points on the components' temperature has been reported. Finally, 3-D FEA is used to conduct heat flow path and heat generation density.

Keywords: Flux Switching Machine, Cooling System, Computational Fluid Dynamics, Finite Element Analysis, Thermal Analysis.

1 Introduction

RESEARCH on electric vehicles (EVs) has been one of the hottest topics in recent years due to the increasing focus on sustainable energy and environmental preservation [1, 2]. Among permanent magnet (PM) machines, flux switching PMs (FSPMs) are suited in renewable energy [3] especially EV [4] applications thank to the great advantages such as high torque density, simple structure, high efficiency, and easy integration with other mechanical components [5-8]. These merits can be enhanced utilizing the topology of axial field [9] flux switching PM (AFFSPM) which are rotor-PM as low total harmonic distortion, and slight cogging torque are achieved [10]. However, AFFSPM suffer from demagnetization issue of PMs [11].

Winding resistance and copper losses both increase with temperature, leading to diminished efficiency and compromised winding insulation [12]. There is also a negative correlation between temperature and the remanent flux density and corrective force of a PM [13, 14]. This results in a decline in PM strength and a consequent decrease in the torque density of PM machines [15, 16]. Recently, the thermal analysis of PM machines has been the subject of a significant amount of research. Thermal research of AFFSPM is of utmost significance due to the fact that, in contrast to FSPMs, the circulation of heat within AFFSPM is entirely distinct [17]. Thermal analysis can be conducted using analytical and numerical approaches. The Lumped Parameter Model (LPM) is a fast-calculating analytical approach for estimating the mean temperature [18]. Using analytical relationships, 3-D LPMs for axial flux [18] and radial flux [19, 20] FSPMs with different

Iranian Journal of Electrical & Electronic Engineering, 2024.
Paper first received 12 June 2023 and accepted 16 February 2024.
* The authors are with the Faculty of Electrical Engineering, Shahid Beheshti University, Tehran, Iran.
E-mails: alizarghani.97@gmail.com, pedram.dehgosha@gmail.com, h_torkaman@sbu.ac.ir, and a_ghaheri@sbu.ac.ir.
Corresponding Author: H. Torkaman.

topologies were presented. On the other hand, numerical approaches like finite element analysis (FEA) and computational fluid dynamics (CFD) have found widespread application due to capability of temperature distribution approximation in all components.

FEA is excellent at simulating heat transfer in natural cooling system which are used in thermal analysis of FSPMs [21, 22]. More accurate modelling of airflow within the machine allows for more in-depth convective heat transfer analysis from machine components to the cooling system, which is possible using CFD. Analyzing cooling systems, modelling ventilation, and calculating convection coefficients are some applications of CFD [23]. By using CFD modelling to test the effect of adding copper bars as additional heat transfer channels between the stator teeth and the liquid cooling chamber in the end shield, it was shown in [24] that a temperature reduction of up to 15% was possible. As internal heat transfer of electric machines varies with the topology, it is necessary to perform thermal analysis for a unique configuration. In conventional FSPMs, PMs are located in the stator-side whereas for AFFSPM, PMs are transferred from the stator-side to the rotor-side. Moreover, in AFFSPM the rotor is segmented and the PMs are embedded between the rotor segments, as opposed to other types of axial flux PMs in which the PMs are positioned on the rotor disc surface [25-27]. CFD is utilized for an in-depth understanding of the heat transfer within the AFFSPM, which is housed in an encased housing with blades to improve efficiency. The impact of housing materials, external heat transfer coefficients, ambient temperature, and various loading and rotational speed conditions on the components' temperature are investigated.

This paper employs both numerical methods (CFD and FEA) to evaluate the thermal performance of a 2.3 kW AFFSPM. In doing so, the temperature distribution, characterization of heat transfer, analysis of fluid flow patterns, thermal performance assessment, and validation and optimization of the design are all accomplished. These goals collectively aim to enhance the efficiency, reliability, and thermal management of the AFFSPM. Electromagnetic losses have been precisely calculated thanks to the application of 3-D FEA. Then, aluminum and cast iron are tested in a thermal study of the chamber, in which the performance of these materials is studied. Besides, the effect of the external convection heat transfer coefficient on the temperature difference of the ATFFSPM' components has been investigated. In addition, the thermal performance will be assessed under different operating conditions, and the distribution of heat generation density and heat flow path inside the interior area will be analyzed. Finally, some suggestions are provided for further improvement in thermal performance. The rest of this paper is organized as follow: in Section 2, the topology of AFFSPM is presented. Electromagnetic losses are derived using 3-D FEA and copper are calculated using temperature-dependent correlation in Section 3. Finally, Section 4 devotes to thermal modeling and thermal analysis of AFFSPM under nominal condition. Also, temperature distribution under various operational condition, and external heat transfer coefficient with two different materials of housing will be performed.

2 Topology of AFFSPM

Fig. 1 depicts the three-dimensional geometry of an AFFSPM, which includes two independent segmented rotors, a double-sided stator, concentrated windings, housing, and PMs. The housing is equipped with blades for better cooling.

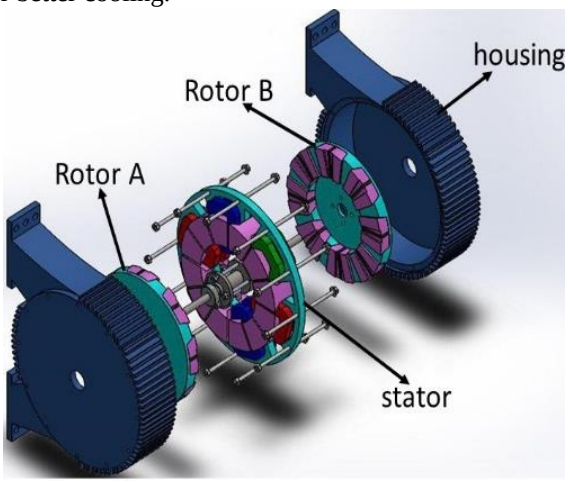

Fig. 1 3-D exploded view of AFFSPM machine.

The segmented rotor has 8 poles and in order to accommodate the PMs, a gap is made between the rotor poles, as shown in Fig. 2(a). Fig. 2(b) depicts the stator core, which comprises of six primary poles and six auxiliary poles with tightly wound coils around the primary poles. The stator also has to be held in position with the help of a support.

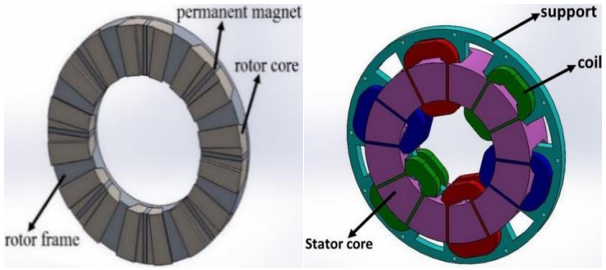

(a) (b)

Fig. 2 Arrangement of (a) rotor-side and (b) stator-side components of AFFSPM.

The nominal specifications of AFFSPM are listed in Table 1. As shown in Fig. 3, the initial stage of the simulation process is to calculate the electromagnetic and copper losses by means of an analytical equation and FEA, respectively. In the interim, mesh generation, boundary conditions, and fluid specifications are established, and a CFD model is developed. The FEA-obtained loss densities are then incorporated into CFD to account for heat generated in components. In addition, the CFD results are compared with FEA results in Ref. [18] to confirm its precision. In the end, the thermal analyses are expanded to examine the impact of housing material and different modes of operation on the component's temperature.

Table 1 The nominal specifications of AFFSPM

Parameter	Value	Unit
Rated Power	2.3	kW
Rated speed	500	rpm
Rated current	9.9	A
Current density	4.5	A/mm^2
Number of stator Slot	12	-
Number of rotor-segments	16	-
Air-gap length	0.5	mm
PM width	5	mm
Coil numbers per phase	4	-
Total axial length	103	mm

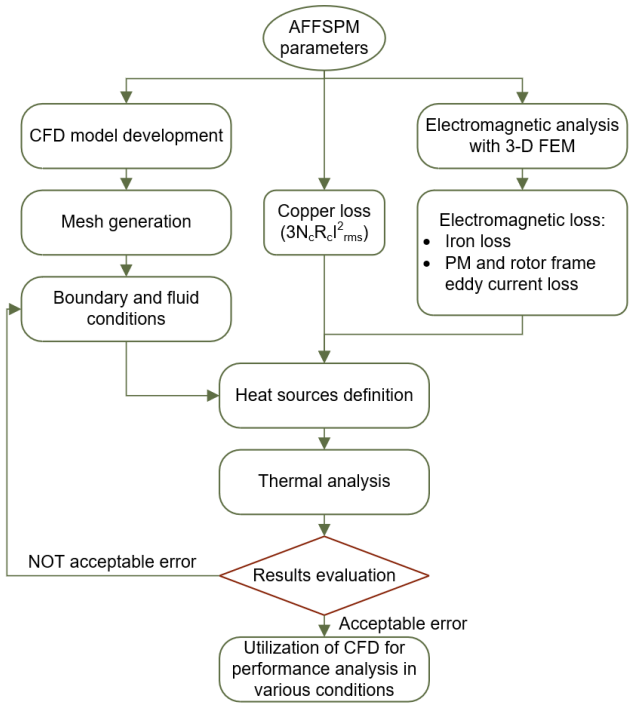

Fig. 3 The process of simulation.

3 Loss Estimation

Losses generate heat, which contributes to an increase in the temperature of the component. Therefore, the first step in performing thermal analysis is to complete the appropriate calculations to determine the power losses. In general, losses occur in the rotor core, stator core, PMs and winding. Because the AFFSPM operates in low-speeds, mechanical losses can be ignored. FEA is used to automatically estimate electromagnetic losses with high precision [28], since the analytical strategy for estimating electromagnetic losses using mathematical correlations requires a large number of assumptions and delivers low accuracy. It should be mentioned that coil resistance is calculated based on temperature dependent empirical correlation as:

$$R_c = R_0[1 + \alpha_T(T_c - T_0)] \quad (1)$$

where R_0 (Ω) is coil resistance in initial temperature, α_T is temperature coefficient, T_c (℃) is the temperature in operating point, and T_0 (℃) is initial temperature. Considering T_c as critical temperature of 150 ℃, the R_c is estimated as 0.36 Ω. Hence, copper losses are derived:

$$P_c = 3N_cR_cI^2_{rms} \quad (2)$$

here, N_c is the number of coils of each phase and I_{rms} (A) is the RMS value of the nominal current.

The axial, radial, and circumferential orientations of the flux path in AFFSPM necessitated the development of a 3D model to improve the precision of the analysis. The losses of laminated magnetic cores, such as the stator core and rotor segments, may be quickly calculated using a post-processing method in FEA. The iron loss density distribution the stator core and rotor segments are depicted in Fig. 4. It can be noticed that the stator teeth's tips and the air-gap face of the rotor segments suffer from large iron loss density compared to other surfaces. Also, the maximum value of core loss distribution in rotor segments is higher than stator core.

Joule losses in the unlaminated components were also calculated. Fig. 5 pictures the eddy current loss density in the rotor frame and PM. As can be observed, the maximum value of eddy current loss density is associated with the locations of in front of the air-gap for both carrier and PM. Because the rotor is segments, leakage flux will be induced to the rotor frame which result in considerable joule loss density. The power losses values are presented in Fig. 6. Of all the losses, the copper losses accounts for the largest proportion with 53%, followed by rotor frames loss with 30%. Considerable amount of rotor frames loss will lead to drop in efficiency. The eddy current loss in PMs is the lowest which is 18.25 W.

Loss sources calculated in this section will be coupled to thermal analysis as heat sources.

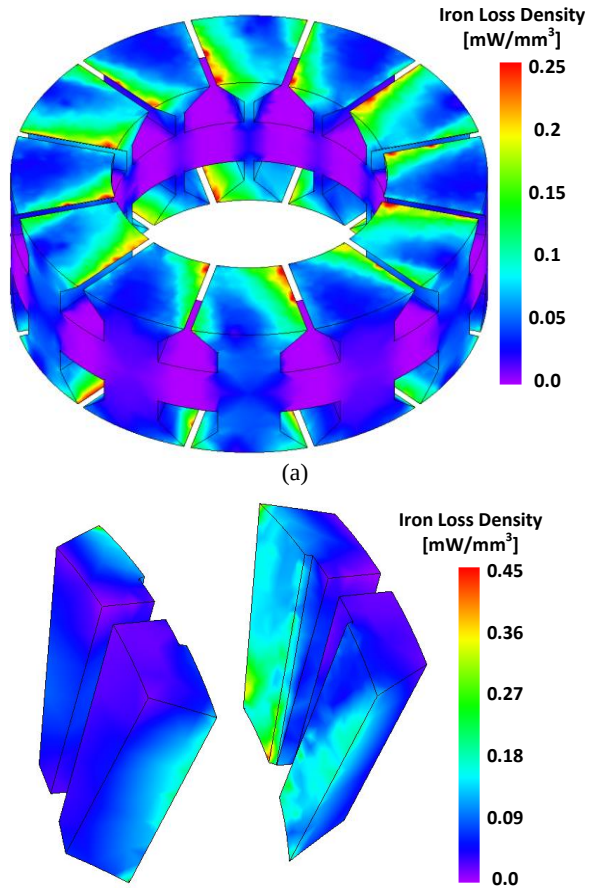

Fig. 4 Iron loss density in (a) stator core and (b) rotor pole.

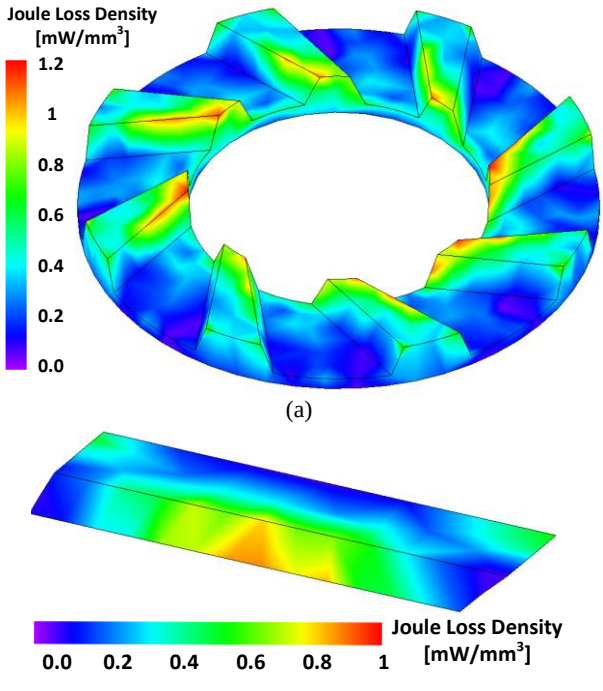

Fig. 5 Joule loss density in (a) rotor frame and (b) PM.

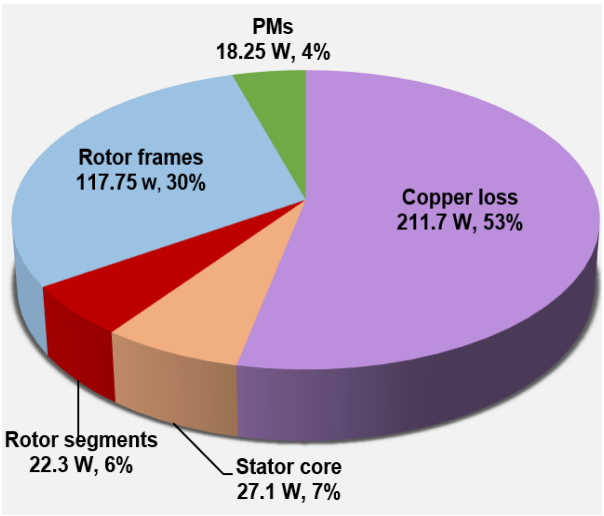

Fig. 6 The value and portion of the loss in various components.

4 Thermal Analysis of AFFSPM

This section devotes to thermal modelling and analysis of AFFSPM. Thermal analysis requires the identification of the density, specific heat capacity, and thermal conductivity of materials. The thermal properties of AFFSPM materials are listed in Table 2.

Table 2 Thermal properties of the AFFSPM components

Component (material)	Thermal conductivity $(\frac{W}{m.\,℃})$	Specific heat $(\frac{J}{kg}℃)$	Density $(\frac{kg}{m^3})$
Winding (copper)	386	380	8954
Support& Rotor frame (aluminum)	237	903	2700
Fluid (air)	0.024	1006	1.225
Housing (cast-iron)	55	456	7920
PM (Nd-Fe-B)	8.95	501.6	7500
Stator& Rotor core (50JN400)	30	450	7650
Shaft (S45C)	49.8	486	7850

The thermal study of the RE-AFSPM has been performed with great precision using Ansys Fluent, one of the most capable CFD tools. Because losses generate heat, the calculated nominal losses from the preceding section are incorporated into the steady-state thermal analysis. The ambient temperature is set to 50 °C to produce the most challenging operating conditions. The steady-state analysis evaluates the temperature distribution of aluminum and cast-iron housings. The assumptions made for the air-fluid are including Newtonian fluid, compressible fluid, non-slip conditions, and fixed properties. The following equations express the relationship between conservation, continuity,

momentum, and energy in a fluid:

$$\frac{\partial u}{\partial x}+\frac{\partial v}{\partial y}+\frac{\partial w}{\partial z}=0 \tag{3}$$

$$\rho_f\left(u\frac{\partial u}{\partial x}+v\frac{\partial u}{\partial y}+w\frac{\partial u}{\partial z}\right)= -\frac{\partial P}{\partial x}+\mu_f\left(\frac{\partial^2 u}{\partial x^2}+\frac{\partial^2 u}{\partial y^2}+\frac{\partial^2 u}{\partial z^2}\right) \tag{4}$$

$$\rho_f\left(u\frac{\partial v}{\partial x}+v\frac{\partial v}{\partial y}+w\frac{\partial v}{\partial z}\right)= -\frac{\partial P}{\partial y}+\mu_f\left(\frac{\partial^2 v}{\partial x^2}+\frac{\partial^2 v}{\partial y^2}+\frac{\partial^2 v}{\partial z^2}\right) \tag{5}$$

$$\rho_f\left(u\frac{\partial w}{\partial x}+v\frac{\partial w}{\partial y}+w\frac{\partial w}{\partial z}\right)= -\frac{\partial P}{\partial z}+\mu_f\left(\frac{\partial^2 w}{\partial x^2}+\frac{\partial^2 w}{\partial y^2}+\frac{\partial^2 w}{\partial z^2}\right) \tag{6}$$

$$\rho_f C_{pf}\left(u\frac{\partial T_f}{\partial x}+v\frac{\partial T_f}{\partial y}+w\frac{\partial T_f}{\partial z}\right)= k_f\left(\frac{\partial^2 T_f}{\partial x^2}+\frac{\partial^2 T_f}{\partial y^2}+\frac{\partial^2 T_f}{\partial z^2}\right) \tag{7}$$

where P is the pressure, ρ_f is the fluid density, μ_f is the fluid absolute viscosity, C_{pf} is the fluid specific heat capacity, and k_f is the thermal conductivity of the fluid. The energy equation for a solid body is as follows:

$$\rho_s C_{ps}\frac{\partial T_s}{\partial t}=k_s\left(\frac{\partial^2 T_s}{\partial x^2}+\frac{\partial^2 T_s}{\partial y^2}+\frac{\partial^2 T_s}{\partial z^2}\right)+\dot{q} \tag{8}$$

where ρ_s is the solid density, C_{ps} is the solid specific heat, k_s is the solid thermal conductivity, and $\dot{q}$ is the rate of solid heat production. The amount of heat flow from the machine's surface to the surrounding environment may be calculated using the convective heat transfer relationship, which is given as:

$$-k\frac{\partial T}{\partial x}=h_{out}\left(T_{H,out}-T_{A,out}\right) \tag{9}$$

here $T_{H,out}$ is the housing surface temperature, $T_{A,out}$ is temperature of the ambient, and h_{out} is the convection heat transfer coefficient. Sensitivity analysis have been performed for the values of h_{out} equal to 10, 20, 40, and 80 $\frac{W}{m^2k}$. The convergence requirement for the energy equation and the coherence for the iterations to reach the remainder are 10^{-6} and 10^{-3}, respectively.

4.1 Effect of the Material of Housing

The temperature distribution in an AFFSPM operating at a nominal speed of 500 rpm is illustrated in Fig. 7. The housings utilized are aluminum and cast iron. It is important to mention that h_{out} is 10 $W/(m^2k)$ and the temperature of ambient is 50 °C. The temperature range of components in the aluminum housing is 136 °C to 187 °C, whereas under identical conditions, the temperature range for the cast iron housing is 137 °C to 191 °C. In contrast, the temperature of the internal fluid in the vicinity of the housing and the rotating components was reduced by 6% when an aluminum housing was utilized. Hence, it can be asserted that the heat transfer characteristics of aluminum housing surpass those of cast-iron housing. Additionally, heat dissipation is enhanced when an aluminum enclosure is utilized. Based on the temperature distribution and the planes Y = 0 and Z = 0, Fig. 7 illustrates that the windings contain the hot point, while the rotor segments exhibit the lowest temperature. The low temperature of the rotor was predicted due to the fact that its loss was lower than that of the stator and copper. Furthermore, they avoid the danger of PM demagnetization by transferring PMs to the rotor side, as opposed to conventional FSPMs in which PMs are located on the stator side. In order to compare the temperature performance of aluminum and cast-iron, a thermal analysis is necessary due to the fact that torque density is dependent on current density. Convection coefficients are not influenced by current density, whereas copper losses increase significantly with current density. As the current density increases, there is a corresponding increase in heat generation within the AFFSPM. As a result, the temperature of every component increase, particularly the windings. As the current density rises from 3.6 A/mm^2 to 6.3 A/mm^2, the average torque experiences a 45% improvement. However, in the process, the PM temperature and winding temperature both increase by 84% and 98%, respectively. An examination of the mean temperatures of the components in Fig. 8 indicates that an increase in current density corresponds to a temperature increase for each component. Additionally, the results indicate that AFFSPM operated at lower temperatures when aluminum housing was utilized as opposed to cast iron housing.

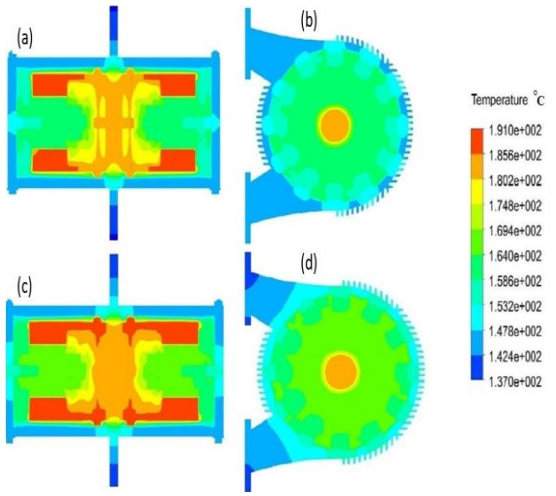

Fig. 7 Temperature distribution at 500 rpm with ambient temperature of 50 ℃ for aluminum housing in (a) plane Y=0, (b) plane Z=0; For cast iron housing in (c) plane Y=0 and (d) plane Z=0.

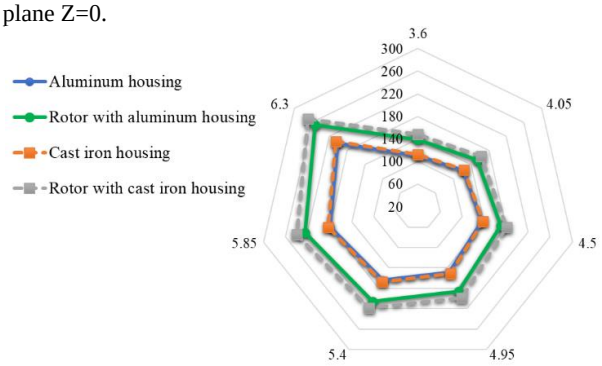

Fig. 8 Analysis of the rotor and housing temperatures versus current density for different housing material.

4.2 Effect of the Ambient Temperature

Fig. 9 temperature mapping for the aluminum housing at 300 K ambient temperature is examined. In the interim, the rotational speed (500 rpm) and h_{out} (10 $W/(m^2k)$) remain constant. Upon comparing the results presented in Fig. 7 and Fig. 9, it becomes evident that a hotspot temperature decreases by approximately 14% for every 46% reduction in ambient temperature.

A comparison is made between the CFD results and the 3-D FEA results presented in [18] to validate the obtained temperature results. The maximum deviation between them in PM is nearly 5.5%, and the error in the winding, which is the most temperature-sensitive component, is only 0.4%, demonstrating that the discrepancy between the methodologies is acceptable. Considering the lower ambient temperature of 2 °C and the longer axial length of the housing in [18], which resulted in improved heat dissipation and, consequently, lower temperatures, are the primary causes of the greater difference in PM temperature.

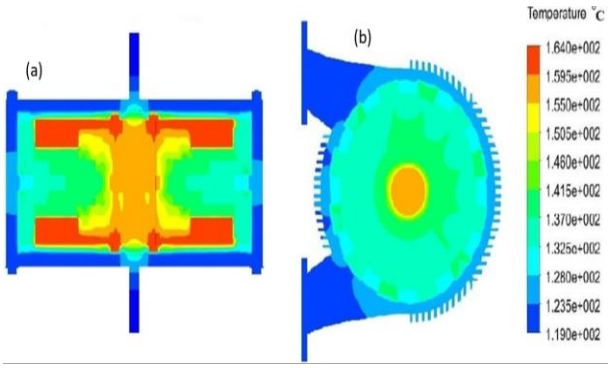

Fig. 9 Temperature distribution at 500 rpm and $h_{out} = 10\ W/m^2k$ with an ambient temperature of 300 K in (a) plane Y=0 and (b) plane Z=0.

Table 3 Temperature comparison between CFD and FEA

Component	CFD	FEA [18]
Winding	164	163.3
Stator	157.2	153
PM	129.4	122.6

4.3 Effect of the Current Density and Rotational Speed

Through the examination of the machine's thermal response at various operating points, one can ascertain that the temperature remains within acceptable thresholds, thereby preserving reliable operation and preventing possible damage. Furthermore, the performance and lifespan of the machine can be assessed through thermal analysis under various operational conditions. Additionally, the identification of potential hotspots or regions susceptible to thermal stress allows for the implementation of design modifications or thermal management techniques that increase the lifespan. Therefore, thermal analysis is performed under various current density and speed conditions in order to identify the safe operating temperature range and ascertain the ideal operating point of the AFFSPM. Concerning this matter, the temperature range observed in the winding and PM is illustrated in Fig. 10. The current density varies between 3.6 A/mm^2 and 6.3 A/mm^2, while the rotational speed differs from 350 to 900 rpm. The rate of temperature increase with current density is greater than that with rotational speed, as the increase in heat transfer coefficients at high velocities results in greater heat dissipation. Furthermore, to enhance the thermal performance of AFFSPM, additional modifications are recommended, such as the development of a cooling system, structural adjustments to the rotor frame, selection of an appropriate material for the rotor frame, and optimization of the stator yoke to minimize core losses, due to the elevated temperatures in both the winding and PM in overspeed and overload conditions.

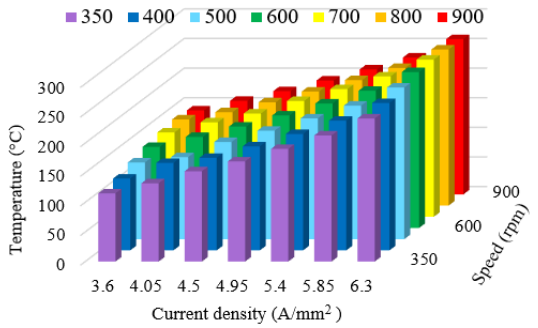

(a)

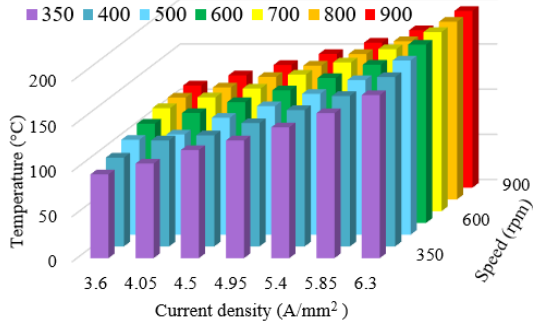

(b)

Fig. 10 Effect of the current density and rotational speed on the temperature of (a) winding and (b) PM.

4.4 Effect of the External Heat Transfer Coefficient

In order to examine the impact of the external convection coefficient on the temperature of components, simulations are performed under different outer convection coefficient values. Various exterior convection coefficient values, including h_{out}=20 $W/(m^2k)$, h_{out}=40 $W/(m^2k)$, and h_{out}=80 $W/(m^2k)$, are simulated to ascertain the impact of these values on the temperature of machine components. The aluminum enclosure functions at the same temperature of 300 K as its outer boundary condition. The outcomes of the temperature distribution on the Y=0 and Z=0 planes are illustrated in Fig. 11. Upon comparing the results, it becomes apparent that an increase in the value of h_{out} led to a corresponding reduction in the temperature of the components. This can be attributed to the fluid's improved capacity for heat dissipation. According to Fig. 11, the temperature range for h_{out}=20 $W/(m^2k)$ is 66 °C to 116 °C. As shown in Fig. 9, the temperature range was 119 °C to 164 °C when h_{out}=10 $W/(m^2k)$. By doubling the value of h_{out}, the maximum temperature has been reduced by 29%. Furthermore, under the condition h_{out}=40 $W/(m^2k)$, the temperature range is 44 °C to 92 °C. Conversely, under the condition h_{out}=80 $W/(m^2k)$, the temperature range is 33 °C to 80 °C. The temperatures decreased by 29%, 43.9%, and 51%, respectively, at h_{out}=30 $W/(m^2k)$, h_{out}=40 $W/(m^2k)$, and h_{out}=80 $W/(m^2k)$, in comparison to h_{out}=10 $W/(m^2k)$.

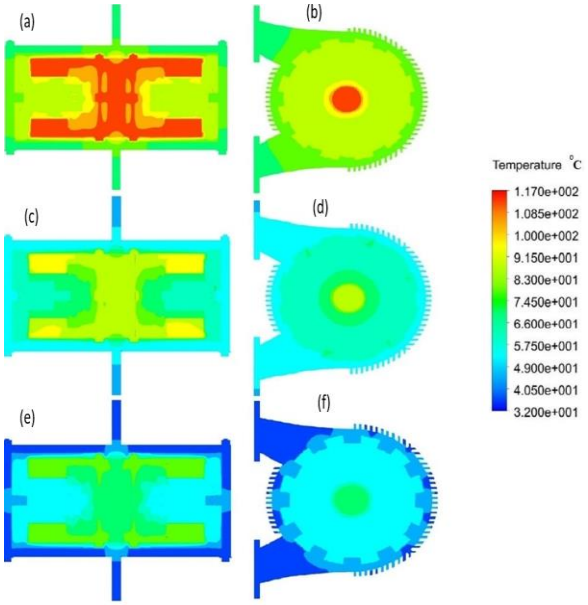

Fig. 11 Temperature distribution at ambient temperature of 300 K for (a-b): $h_{out} = 20$, (c-d): $h_{out} = 40$, and (e-f): $h_{out} = 80$.

Fig. 12 provides a visual representation of the paths that heat transfers through AFFSPM. It can be observed that main heat flux inside AFFSPM is from airgap. Because heat transfers from hot areas to cold regions, most of heat generated by windings and stator core is transferred to the rotor-side through air-gap. In thermal modelling, the density of heat production corresponds to the density of loss in magnetic field analysis. As was previously exhibited, rotor frame loss density was considerable compared to cores. Consequently, the highest value of the localized heat generation density is associated with the rotor frame, as displayed in Fig. 13, because there are more changes in the magnetic field at that location over time compared to other locations.

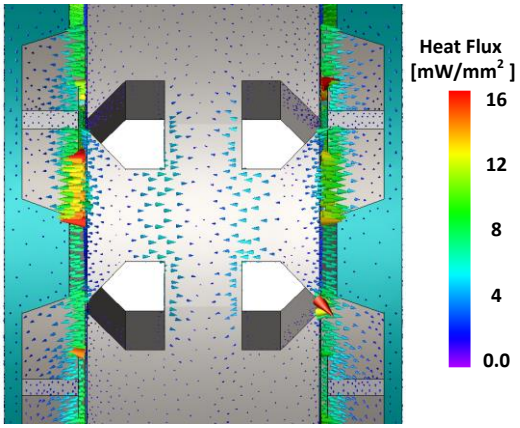

Fig. 12 Heat flux path inside AFFSPM in axial view.

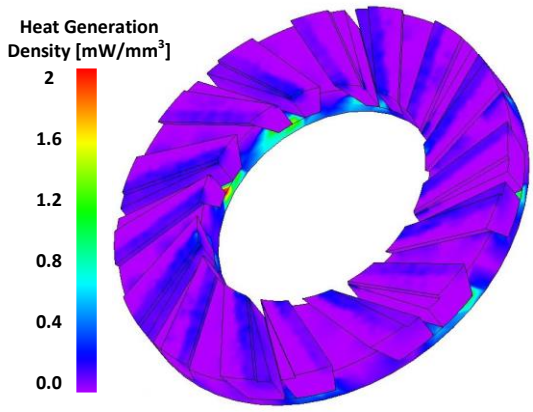

Fig. 13 Heat generation density distribution in AFFSPM.

5 Conclusion

This paper conducted FEA and CFD techniques to analyze the losses and thermal behavior of AFFSPM machine. In 3-D FEA it was concluded that large stray losses are induced in rotor frame. Afterwards, the temperature of the components was lowered by installing blades on the housing, which increased their contact with the surrounding air. Also, two different materials were evaluated to investigate thermal performance. The rotor temperature was lowered by 6% through employing an aluminum housing instead of a cast-iron one. As a result, aluminum housing provides superior heat transmission compared to cast iron. By analyzing the correlation between the maximum temperature and the ambient temperature, it was determined that a decrease of 46% in the ambient temperature would result in a 14% decrease in the highest temperature. Through a range of loading and speed conditions it was shown that thermal problems will occur in overload and overspeed. Hence, some suggestions were presented to reduce losses and enhance heat dissipation capacity. External convection coefficient variation's impact on components' thermal states was also studied. It was obtained that in comparison to external convection coefficient of $10\,W/(m^2k)$, for maximum convection coefficients equal to $20\,W/(m^2k)$, $40\,W/(m^2k)$, and $80\,W/(m^2k)$, the maximum temperature decreased by 29%, 43.9% and 51%, respectively. By changing the current density, it was demonstrated that components can be kept at a lower temperature employing an aluminum housing as opposed to the cast iron.

References

[1] F. Farrokh, A. Vahedi, H. Torkaman, and M. Banejad, "Design and comparison of dual-stator axial-field flux-switching permanent magnet motors for electric vehicle application," *IET Electrical Systems in Transportation*, vol. 13, no. 2, p. e12074, 2023.

[2] J. Faiz and M. Maktobian, "Performance Enhancement of Flux Switching Motor for Electric Vehicle Applications: An Overview," *IET Electrical Systems in Transportation*, vol. 2024, p. 9071667, 2024.

[3] A. Darjazini, A. Vahedi, S. Gharehseyed, and A. Nobahari, "A modified approach for efficient cogging torque suppression in a flux switching permanent magnet generator used in micro-scale wind turbines," *IET Electric Power Applications*, 2023.

[4] W. Yu, W. Hua, and Z. Zhang, "Cooling Analysis of High-Speed Stator-Permanent Magnet Flux-Switching Machines for Fuel-Cell Electric Vehicle Compressor," *IEEE Transactions on Vehicular Technology*, vol. 71, no. 1, pp. 210-219, 2021.

[5] A. Ghaheri, E. Afjei, and H. Torkaman, "Design optimization of a novel linear transverse flux switching permanent magnet generator for direct drive wave energy conversion," *Renewable Energy*, vol. 198, pp. 851-860, 2022.

[6] E. F. Farahani, N. J. Baker, and F. Mahmouditabar, "An Innovative H-Type Flux Switching Permanent Magnet Linear Generator for Thrust Force Enhancement," *Energies*, vol. 16, no. 16, p. 5976, 2023.

[7] L. Shao, R. Navaratne, M. Popescu, and G. Liu, "Design and Construction of Axial-Flux Permanent Magnet Motors for Electric Propulsion Applications—A Review," *IEEE Access*, vol. 9, pp. 158998-159017, 2021.

[8] A. Ghaheri, E. Afjei, and H. Torkaman, "A novel axial air-gap transverse flux switching PM generator: Design, simulation and prototyping," *IET Electric Power Applications*, vol. 17, no. 4, pp. 452-463, 2023.

[9] A. Ghaheri, A. Mohammadi Ajamloo, H. Torkaman, and E. Afjei, "Design, modelling and optimisation of a slot-less axial flux permanent magnet generator for direct-drive wind turbine application," *IET Electric Power Applications*, vol. 14, no. 8, pp. 1327-1338, 2020.

[10] H. Torkaman, A. Ghaheri, and A. Keyhani, "Design of rotor excited axial flux-switching permanent magnet machine," *IEEE Trans. Energy Convers.*, vol. 33, no. 3, pp. 1175-1183, 2018.

[11] H. Torkaman, A. Ghaheri, and A. Keyhani, "Axial flux switched reluctance machines: a comprehensive review of design and topologies," *IET Electric Power Applications*, vol. 13, no. 3, pp. 310-321, 2019.

[12] M. Farahzadi, K. Abbaszadeh, and S. Mirnikjoo, "Electromagnetic-Thermal Analysis of a Hybrid-Excited Flux Switching Permanent Magnet Generator for Wind Turbine Application," *IEEE Transactions on Energy Conversion*, pp. 1-12, 2023.

[13] F. Mahmouditabar, A. Vahedi, and N. Takorabet, "Design and analysis of interior permanent magnet

motor for electric vehicle application considering irreversible demagnetization," *IEEE Transactions on Industry Applications*, vol. 58, no. 1, pp. 284-293, 2021.
[14] F. Mahmouditabar, A. Vahedi, and F. Marignetti, "The Demagnetization Phenomenon in PM Machines: Principles, Modeling, and Design Considerations," *IEEE Access*, vol. 11, pp. 47750-47773, 2023.
[15] G. Davarpanah, J. Faiz, H. Shirzad, and M. Lotfizadeh, "A Modular Hybrid Excited Switched Reluctance Motor with Two Groups of Permanent Magnets to Enhance the Performance of the Motor," *IEEE Transactions on Energy Conversion*, pp. 1-12, 2024.
[16] A. Zarghani, A. Ghaheri, M. Abolghasemi, E. Afjei, and H. Torkaman, "Thermal Modeling and Analysis of Transverse-Radial Flux Magnetic Gear," in *2023 3rd International Conference on Electrical Machines and Drives (ICEMD)*, 20-21 Dec. 2023 2023, pp. 1-7, doi: 10.1109/ICEMD60816.2023.10429212.
[17] D. A. Howey, P. R. Childs, and A. S. Holmes, "Air-gap convection in rotating electrical machines," *IEEE Transactions on Industrial Electronics*, vol. 59, no. 3, pp. 1367-1375, 2010.
[18] A. Zarghani, H. Torkaman, N. Arbab, and M. S. Toulabi, "Lumped parameter thermal network for thermal analysis of a rotor-excited axial flux switching machine with electromagnetic-thermal design," *Measurement*, vol. 193, p. 110971, 2022.
[19] X. Cai, M. Cheng, S. Zhu, and J. Zhang, "Thermal modeling of flux-switching permanent-magnet machines considering anisotropic conductivity and thermal contact resistance," *IEEE Transactions on Industrial Electronics*, vol. 63, no. 6, pp. 3355-3365, 2016.
[20] A. Zarghani, M. Farahzadi, A. Ghaheri, K. Abbaszadeh, H. Torkaman, and E. Afjei, "2D Lumped Parameter Model for Temperature Prediction in a Radial Flux Switching Generator with Two Permanent Magnet Types," in *2023 3rd International Conference on Electrical Machines and Drives (ICEMD)*, 20-21 Dec. 2023 2023, pp. 1-6, doi: 10.1109/ICEMD60816.2023.10429503.
[21] A. Zarghani, S. M. Saghin, A. Ghaheri, E. Afjei, and H. Torkaman, "Magneto-Thermal Analysis of a Novel Excited Outer Rotor Flux-Switching PM Machine," in *14th Power Electronics & Drives: Systems and Technologies Conference (PEDSTC)*, Babol, Iran, 31 Jan.-2 Feb. 2023 (2023), pp. 1-6.
[22] G. Zhang, W. Hua, M. Cheng, B. Zhang, and X. Guo, "Coupled magnetic-thermal fields analysis of water cooling flux-switching permanent magnet motors by an axially segmented model," *IEEE Transactions on Magnetics*, vol. 53, no. 6, pp. 1-4, 2017.
[23] P. Dehgosha, A. Zarghani, H. Torkaman, and A. Ghaheri, "Three-Dimensional Thermal Analysis of a Rotor-Excited Axial Flux Switching Permanent Magnet Machine by Computational Fluid Dynamics Method," in *2023 3rd International Conference on Electrical Machines and Drives (ICEMD)*, 20-21 Dec. 2023 2023, pp. 1-6, doi: 10.1109/ICEMD60816.2023.10429151.
[24] Y. C. Chong, E. J. E. Subiabre, M. A. Mueller, J. Chick, D. A. Staton, and A. S. McDonald, "The ventilation effect on stator convective heat transfer of an axial-flux permanent-magnet machine," *IEEE Transactions on Industrial Electronics*, vol. 61, no. 8, pp. 4392-4403, 2013.
[25] D. A. Howey, A. S. Holmes, and K. R. Pullen, "Measurement and CFD prediction of heat transfer in air-cooled disc-type electrical machines," *IEEE Transactions on Industry Applications*, vol. 47, no. 4, pp. 1716-1723, 2011.
[26] L. Veg and J. Laksar, "Comparison of two types of cooling of axial flux permanent magnet machines by CFD simulation," in *2019 International Conference on Electrical Drives & Power Electronics (EDPE)*, 2019: IEEE, pp. 303-306.
[27] J. Li, Y. Lu, Y.-H. Cho, and R. Qu, "Design, analysis, and prototyping of a water-cooled axial-flux permanent-magnet machine for large-power direct-driven applications," *IEEE Transactions on Industry Applications*, vol. 55, no. 4, pp. 3555-3565, 2019.
[28] R. Nasiri-Zarandi, A. Ghaheri, and K. Abbaszadeh, "Thermal Modeling and Analysis of a Novel Transverse Flux HAPM Generator for Small-Scale Wind Turbine Application," *IEEE Transactions on Energy Conversion*, vol. 35, no. 1, pp. 445-453, 2019.

Ali Zarghani was born in Mashhad, Iran, in 1997. He received a B.S. degree from the University of Birjand, Birjand, Iran, in 2018 and a M.S. degree from Shahid Beheshti University, Tehran, Iran, in 2021, both in power electrical engineering. Since 2021, he has been a research assistant in the faculty of electrical engineering at Shahid Beheshti University, Tehran, Iran. His research interests include analytical and finite element method development for multi-physics (electromagnetic, thermal, and mechanical) design, modeling, analysis, optimization, and manufacturing of various electromagnetic devices, with a focus on radial and axial flux PM machines for transportation and renewable energy applications.

Pedram Dehgoshaei received the B.S. degree in electrical engineering from Azad University, Shiraz, Iran in 2009 and the M.Sc. degree in Power Electronic and Electrical Machines engineering from Shahid Beheshti University, Tehran, Iran in 2019. His research interests include the transient

and steady-state thermal analysis of electrical machines, magnetic analysis and the use of optimization algorithms in the design of electrical machines.

Hossein Torkaman (Senior Member, IEEE) is currently an Associate Professor with the Faculty of Electrical Engineering, Shahid Beheshti University, Tehran, Iran. He has published more than 160 technical papers in journal articles and conference proceedings, and four issued patents. He is the author of five books. He was a recipient of different awards and funds from university and companies. He is the Head of the electric machines, power electronic, and motor drives research center laboratory. His main research interests include power electronics, electrical machines, and renewable energies.

Aghil Ghaheri received the B.Sc. degree in electrical engineering from Shahrood University of Technology, Shahrood, Iran, in 2014, and the M.Sc. and Ph.D. degrees in electrical engineering from Shahid Beheshti University, Tehran, Iran, in 2016 and 2022, respectively, where he is currently working as a postdoctoral researcher at the Power Electronics and Motor Drives Laboratory. His research interests include permanent magnet and switched-reluctance machines, magnetic gears, and wireless power transfer systems. He has a strong focus on BLDC, flux switching, transverse flux, Axial field PM Synchronous, flux modulated machines, coaxial magnetic gears, and PCB motors for renewable energy, automotive and household applications. His expertise is Finite Element Analysis, Analytical Modelling, Optimization, manufacturing, and test of electrical machines.